Journal of Energy Storage 32 (2020) 101699

Contents lists available at ScienceDirect

Journal of Energy Storage

journal homepage: www.elsevier.com/locate/est

New prominent lithium bromide-based composites for thermal energy storage

Emilie Courbon[a,*], Pierre D'Ans[b], Oleksandr Skrylnyk[a], Marc Frère[a]

[a] Department of Thermodynamics and Mathematical Physics, Université de Mons, Boulevard Dolez 31, B-7000 Mons, Belgium
[b] 4MAT Department, Université libre de Bruxelles (ULB), Avenue F.D. Roosevelt, 50 - CP 194/3, B-1050 Bruxelles, Belgium

ARTICLE INFO

Keywords:
Lithium bromide
Silica gel
Activated carbon
Water sorption
Thermochemical heat storage

ABSTRACT

Four different LiBr-based composite materials have been synthesized with silica gel or activated carbon as host porous matrix. High salt contents were incorporated in these composites: 37 wt% and 53 wt% for silica gel/LiBr composites; 32 wt% and 42 wt% for activated carbon/LiBr composites. The performance of these materials in conditions representative of the applications of sanitary hot water production and space heating demonstrates the very high potential of the silica gel/LiBr 53 wt% composite. It exhibits an unprecedented energy storage density of 261 kWh/m^3 (adsorption temperature: 30 °C, desorption temperature: 80 °C and water vapor pressure of 12.5 mbar) and of 381 kWh/m^3 when the desorption temperature reaches 120 °C. This promising material presents a good composition homogeneity, high water uptakes between 10 °C and 80 °C, and no measurable loss of sorption properties upon 10 cycles. This composite was tested in an open type laboratory set-up to complete its analysis for heat storage applications, at the scale of 200 g. The best energy storage density reached during 3 h 26 min was as high as 246 kWh/m^3 (adsorption temperature: ~29 °C and water vapor pressure of ~12.5 mbar).

1. Introduction

Thermal heat storage systems for residential applications are currently the center of interest of many researches in order to extend the use of renewable energy resources [1–3]. They help to overcome the mismatch between the availability of the heat source (solar heat, waste heat) and the heat needs of the buildings [4–6]. Among the thermal energy storage technologies, thermochemical heat storage processes are the most promising option, with the highest energy storage densities, and thus the best compactness of the storage system. This criterion is essential for a residential house due to the lack of available space [7–9]. However, this technology still requires many research efforts before a possible market deployment, for the reactor/system design as well as for the materials development [10–12].

One of the main challenges is to develop new thermochemical materials with high energy storage densities [13,14]. Considering seasonal storage for residential heating and hot water production, the annual amount of energy to be stored is high, around 3000 kWh/year for each application, for a 100 m^2 low energy building in Belgium [15]. In order to limit the volume of the storage system, the minimum energy storage density should be 150 kWh/m^3. In this case, the storage volume would be lower than 20 m^3. In the current state-of-the-art, the energy storage densities of the storage materials are measured for residential heating applications, for which the adsorption temperature is low (30 °C). However, for hot water production applications, the adsorption temperature must be higher, around 50–60 °C, which reduces the energy storage density of the materials. The desorption temperature is taken between 80 and 120 °C to permit using solar collectors or waste heat. The energy storage densities of materials are rarely studied in conditions of both applications of residential heating and hot water production. Having a material with high energy density for both temperature conditions would be of interest for the seasonal thermochemical energy storage for building applications. The choice of the storage material is crucial. Its sorption properties must perfectly fit the cycle working conditions of the system in order to optimize its performances [16]. Many efforts are done to develop new energy storage materials with specific properties such as high energy storage density, good stability upon multi-cycles (consecutive adsorption/desorption steps), non-toxicity and cost-effectiveness [17,18]. Thermochemical heat storage used a reversible sorption process. The storage material can be hygroscopic inorganic salts, sorbents or composite materials. As far as sorbents are concerned, silica gels [19,20], activated carbon [21] and zeolites [22] are the most often used, but new sorbents are currently evaluated for the heat storage applications such as aluminophosphates (AlPOs and SAPOs) [23] and Metal Organic Frameworks (MOF) materials [24–26]. The composite materials (hygroscopic salt

* Corresponding author.
E-mail address: Emilie.courbon@umons.ac.be (E. Courbon).

https://doi.org/10.1016/j.est.2020.101699
Received 25 February 2020; Received in revised form 25 June 2020; Accepted 18 July 2020
Available online 07 August 2020
2352-152X/

Nomenclature

A	adsorption potential
AC	activated carbon
BET	Brunauer–Emmett–Teller
BJH	Barett, Joyner and Halenda
C_p	heat capacity
$C_{p,a}$	the dry air heat capacity
DA	Dubinin–Astakhov
d_p	pore diameter (nm)
E	characteristic energy of adsorption
ICP	Inductively coupled plasma
m	mass of the anhydrous composite
$\dot{m}_a$	mass air flow rate through the reactor
MOF	Metal Organic Frameworks
n	constant
P	water vapor pressure (Pa)
P_s	saturation vapor pressure (Pa)
Q	heat of sorption (J/g dry composite)
$\dot{Q}$	specific thermal power
R	gas constant
r_p	pore radius (nm)
RH	relative humidity (%)
SC_{BET}	salt content of composite calculated from BET results
SEM-EDX	Scanning Electron Microscope coupled with energy-dispersive X-ray spectroscopy
SG	silica gel
SWS	Selective Water Sorbent
t	time
t_e	upper integration time limit
T	temperature
V_p	pore volume (cm^3/g)
w	water uptake (g/g)
XRD	X-rays diffraction
XRF	X-rays fluorescence
x_{LiBr}	LiBr content of composite
ΔE	Volumetric energy storage density (kWh/m^3)
$\Delta H_{crucible}$	integration of the heat flow signal during a blank test
ΔH_{exp}	integration of the heat flow signal during the test
ΔH_{is}	isosteric heat of sorption
$\Delta m_{CA-LiBr}^{combust.,\%}$	relative mass loss due to combustion
$\Delta m_{CA-LiBr}^{dehyd.,\%}$	relative mass loss due to dehydration
ΔT	temperature difference
ΔT_a	temperature difference between inlet and outlet conditions
ρ_s	bulk density of the dry composite (kg/m^3)
ρ_{salt}	density of the salt (kg/m^3)

incorporated into the pores of a host matrix) present interesting properties for thermal energy storage applications, with a behavior in-between the inorganic salts and the porous materials. The best advantages of these materials are that the matrix mitigates the problems due to the salt deliquescence, such as agglomeration, free-flowing and corrosion problems [27,28] that could be encountered when using pure salts. The heat and mass transfers are also enhanced in the composite materials [29].

Several salt/matrix pairs have already been tested in the literature. Concerning the porous host matrix, sorbents such as silica gels [30–32], activated carbons [33], zeolites [34–36], MOF [37–39], carbon nanotubes [40] or vermiculite [41] have been studied. In terms of inorganic salts, the main tested salts are $CaCl_2$ [42–44], $MgSO_4$ [35,45], $SrBr_2$ [32,46], LiBr [33,40,47], and LiCl [48,49]. From all the previous works on composite materials, the main outputs could be summarized as follows. The properties of the composites depend on the preparation conditions (dry or wet process, concentration of the aqueous solution [25], time of impregnation, temperature of impregnation) but also on the porous characteristics of the host matrix [50] and the nature of the inorganic salt [51]. Indeed, the water sorption mechanisms are not the same when incorporating the salt in microporous, mesoporous or macroporous matrices. The water sorption mechanism on composite materials may include first the formation of crystalline salt hydrates, followed by the deliquescence of the salt and formation of the salt solution and then absorption by the salt solution. However, the presence of crystalline salt hydrates is not always observed, for example it is not the case when using a microporous matrix. The water sorption capacity is highly dependent on the salt content as the sorption process is mainly due to the salt hydration/dehydration and not to sorption on the porous sorbent [52–54]. The main limitation of the composite material is the risk of leakage of the salt solution formed in case of excessive hydration, which may cause instability issues upon repeated adsorption/desorption cycles and also may provoke corrosion of the metal parts of the reactor when the used salt is corrosive [29,55]. A compromise must be found between a high salt content (to increase the energy storage density) and a good multi-cycles stability (to ensure a reproducible heat storage capacity upon repeated adsorption/desorption cycles) [32].

In the present work, we focused on lithium bromide-based composites. LiBr was mainly used as pure salt for absorption cooling applications [56–59]. The literature on LiBr/H_2O absorption cooling includes a huge amount of theoretical and experimental results. New results concerning refrigeration are still being reported, for example in [60,61]. Asfand and Bourouis chose the water/LiBr pair for their absorption cooling system, using LiBr solution, because of the non-volatility of LiBr sorbent and the high heat of vaporization of water. However, they highlighted the corrosion problems of such a system and the high risk of crystallization [62]. Working with a solution in a storage reactor is not easy to handle and the risk of corrosion of the metallic parts of the reactor is increased. To overcome these drawbacks, the use of a composite material, confining the salt in the pores of a host matrix, is possible. The storage material is then solid, which is easier to handle, and the corrosion issues are limited [63,64]. However, additional care is needed to assure sufficient heat transfer, compared to liquid heat storage.

However, the studies of LiBr/H_2O or LiBr-matrix/H_2O for adsorption heat storage applications are not so numerous. There are few works that investigate the sorption properties and kinetics of composites based on LiBr at a relatively small scale (several mg). However, there is a huge lack of information about the hygrothermal behavior of these materials at a higher scale (>100 g) or so. Even if researches report about the potential of use of the synthesized composites in heating (or cooling) applications, the current state of the art strongly lacks experimental results from laboratory prototypes, while a loss of performance is expected between the characterization tests and the test on prototypes where equilibrium is not reached [65,66].

Several LiBr based composites were already reported in the literature. For example, Gordeeva et al. [33] reported two composites, one based on LiBr and mesoporous synthetic carbon (SWS-2C) and the other one based on LiBr and macroporous expanded graphite (SWS-2EG). The salt contents of these composites were 29 wt% and 33 wt% for SWS-2C and SWS-2EG respectively. The mechanism of water sorption was different in these two composites. In the SWS-2EG, crystalline LiBr and LiBr.H_2O were observed, followed by the formation of LiBr solution, whereas in the SWS-2C, no crystalline hydrate was observed, the solution of LiBr was formed from the beginning of the hydration process. This showed the influence of the matrix porosity on the water sorption behavior of the composites. The results reported by Gordeeva et al. were accented on the sorption properties. The authors cited thermal energy storage as a potential application for this material, but no

experiment in an energy storage prototype was carried out. In [67], Gordeeva at al. studied the methanol sorption properties of composites silica gel/LiCl (31 wt% and 21 wt%) and silica gel/LiBr composites (29 wt% and 24 wt%), all composites synthesized by the dry impregnation process. Authors underlined that the promising adsorption properties could be used along with cooling or heating applications. However, these materials were not investigated yet in a laboratory or large-scale prototype. Grekova et al. [40] studied composites based on multi-wall carbon nanotubes and 3 salts ($CaCl_2$, LiCl and LiBr) for long-term and short-term heat storage. Concerning the composite based on LiBr, the salt content was 42 wt%. For this composite, only the methanol sorption was studied and not the water sorption as it was done for the two other composites. Besides, the heat storage capacities were measured only on small scale samples and not in an experimental heat storage prototype. Haut et al. [68] studied the composites based on LiBr and activated carbon or activated alumina. The salt contents were 8.5 and 13.2 wt% respectively. They adsorb 0.1 g/g and 0.3 g/g of water at 30 °C and 60% of relative humidity (i.e. 25 mbar) respectively. The authors used a fixed bed experimental set-up of 17.7 mL as a bed volume. However, they did not highlight the targeted application of the synthesized composites. Mrowiec-Bialon et al. [69] developed a composite SiO_2-LiBr at 30 wt.% by the sol-gel process and measured the water vapor sorption isotherm at 25 °C. This composite showed a gradual decay of adsorption properties during repeated adsorption/desorption cycles (100 cycles): the $SiO_2/CaCl_2$ composite synthesized by the same sol-gel process is therefore preferred. The authors intended to use the developed composite as a desiccant. The use of mesoporous silica gel as host matrix was done by Gordeeva et al. [47] and Tanashev et al. [70] with the KSKG silica gel. With the dry impregnation process and with LiBr aqueous solution at 35 wt%, 48 wt% and 70 wt%, they obtained composites with salt content of 32 wt%, 43 wt% and 57 wt%, respectively (SWS-2 L). The composite at 57 wt% adsorbs around 0.29 g H_2O/g composite at 40 °C and 13 mbar. The water sorption process includes the formation of solid crystalline monohydrate at low water pressure followed by the absorption by the LiBr solution. The multi-cycles stability for these composites was not evaluated, neither the salt dispersion inside the matrix, nor the presence or absence of salt on the surface of the silica particles for the high salt content.

The goals of the present work consisted in the synthesis and complete characterization of LiBr based composites with silica gel and activated carbon as host matrices, followed by an experimental validation at the scale of 200 g of material. For the first time, the multi-steps incipient wetness process developed in [32,43,71] was applied to LiBr salt for the synthesis of the aforementioned composites. This method allowed the salt content (and thus the energy storage density) to be increased, and the multi-cycle stability to remain high. Moreover, the originality of this work consisted in measuring the water sorption capacities and the energy storage densities of the composites in conditions close to the real applications, such as low temperature heating in the residential sector and hot water production. To do so, the most promising composite for the targeted applications was completely characterized by common laboratory methods and then tested in a specially designed laboratory open-type sorption set-up. The tests performed at the higher sample scale in a laboratory energy storage prototype allowed us to refine the specific thermal power and the energy storage density in practical working conditions. This helped linking directly the performances of the synthesized composite with a designed reactor. Based on these results, the relevance of these composites in thermal energy storage systems for space heating and hot water production applications was discussed.

2. Materials and methods

2.1. Preparation of the composites

The composite materials were synthesized with lithium bromide (99.9%) provided by Sigma Aldrich, with silica gel (SG) provided by Sanpont and with activated carbon SRD10034 (AC) provided by Chemviron.

All the composites were synthesized with the multi-step incipient wetness method already reported in [32,43,71]. Laboratory-scale samples were prepared by firstly drying few grams of the porous matrix (~5 g for SG and ~3 g for AC) in an oven at 200 °C (2h30 for SG and 3 h for AC). A volume of aqueous solution of LiBr at 40 wt% equal to the matrix pore volume was added, the impregnation time was 1 h. Then the sample was dried in the oven at 200 °C for at least 1 h. The impregnation and drying steps were repeated several times to reach the desired salt content (one or two impregnation steps for SG-based composites and two or three impregnation steps for the AC-based composites). The salt content has been obtained by measuring the mass difference between the final sample mass and the anhydrous matrix mass.

The most promising composite was also synthesized at higher scale in order to be tested in a lab-scale prototype. Indeed, 500 g of this composite were produced following an up-scaled synthesis protocol (longer drying time).

2.2. Verification of the salt content

Regarding the salt content determination, the same protocol could not be used for both types of composites. For the SG-based composites, X-ray fluorescence (XRF) was used. Some SG/LiBr was mixed with a boric acid, compressed, dried at 150 °C in a standardized metal vessel and set into the XRF device. The measurement itself was performed using a Pioneer S4 (Brüker) device in “standardless” mode (instrumental error < 0.05%). Since this device is not suitable for light elements (Li, O), the silica gel content was assessed based on the Si measurement, and the salt content, based on the Br measurement. Stoichiometric LiBr and SiO_2 were assumed. Additional measurements were made using digestion in 40% hydrofluoric acid, followed by the analysis of the obtained solution using inductively coupled plasma (ICP, Varian Vista-MPX). With this method, Si and Li concentrations can be measured.

For the AC-based composites, XRF is not suitable due to the absence of any exploitable X-ray peak for C. Instead, the combustion of C in an oxidizing atmosphere was exploited. In a thermo-gravimetric analyzer (TGA-NETZSCH STA 409 PC/PG, with Proteus® software for data treatment), ~35 mg of the studied materials were exposed to a thermal treatment consisting of a heating stage until 500 °C at 1 °C/min, followed by a treatment at constant temperature of 500 °C for 12 h. This treatment was performed under constant dry oxygen flow (60–80 mL/min) and aims at 1) desorbing the residual water; 2) combusting the carbon matrix. The salt mass content (in the dry composite) was obtained by comparison of the mass after water desorption and the mass after carbon combustion. The upper temperature was selected to be slightly below the melting point of LiBr. It was experimentally verified that no mass loss occurs for the salt alone, except dehydration. The LiBr contents were calculated as follows:

$$x_{LiBr} = \frac{100 - \Delta m_{CA-LiBr}^{combust.,\%} - \Delta m_{CA-LiBr}^{dehyd.,\%}}{100 - \Delta m_{CA-LiBr}^{dehyd.,\%}} \times 100 \quad (1)$$

With $\Delta m_{CA-LiBr}^{combust.,\%}$ the relative mass loss due to combustion in% and $\Delta m_{CA-LiBr}^{dehyd.,\%}$ the relative mass loss due to dehydration in%.

2.3. Structural characterization

Crystalline phases were analyzed using a X-ray diffractometer (Brücker D500) in θ/2θ mode, using the Cu Kα ray. LiBr is extremely hygroscopic. In order to detect the salt, prior drying was made overnight (150 °C). AC/LiBr samples were crushed. In addition, a special holder was used to protect the samples from the atmosphere during the

measurement. Moreover, the selected scan rate was quite high to limit the acquisition time to ~20 min.

2.4. Verification of the sample homogeneity

Regarding the salt repartition, cross-sectional analyses were made on several particles of each composite, using a SEM-EDX (FEI, EDAX®), in secondary electrons mode. For the AC-based samples, this was done by impregnating the particles inside Clarocit® (Struers) resin, by polishing the obtained sample and by depositing conductive carbon. For the SG-based samples, the Epofix® resin was used. Elemental mappings of the cross-sections were thus made on all the samples, for the elements that generate an exploitable EDX signal.

2.5. Measurement of the porous characteristics

The porous characteristics were obtained by measuring the nitrogen sorption isotherm at −196 °C using a Belsorp max apparatus and using the BET method. Prior to nitrogen sorption measurements, samples were dried at 150 °C for 10 h. The specific surface area was calculated using the branch in the relative pressure range between 0.05 and 0.3 for SG-based composites and between 0.02 and 0.2 for the AC-based composites. The total pore volume was estimated from the amount adsorbed at relative pressure of 0.99. The average pore diameter was calculated with the hypothesis of cylindrical pores. The pore size distribution was obtained by the Barrett, Joyner and Halenda (BJH) method for the SG-based composites and by the MP-plot method for the AC-based composites, both applied on the nitrogen desorption isotherm. Different methods of pore size distribution determination were used because of the difference of porosity of SG and AC. Indeed, SG is mainly mesoporous whereas AC is mainly microporous. The BJH method is applied for mesoporous materials and cannot be applied for microporous materials for which the MP-plot is preferred.

2.6. Measurement of the energy storage densities: efficiency tests

The efficiency tests were performed on TG-DSC111 or Sensys Evo, both coupled with humidity generator Wetsys from Setaram. These apparatus measure simultaneously the mass uptake or loss and the calorimetric signals. Prior to the measurements, around 50 mg of composite sample were dried at 200 °C for 10 h (heating rate: 1 °C/min) under dry nitrogen. The heat capacity (c_p) was measured between 30 °C and 130 °C with a heating rate of 1 °C/min. Then adsorption steps or desorption steps were measured at different temperatures and at water vapor partial pressure of 12.5 mbar. The mass uptake (or loss) and the heat flow were measured between 30 and 80 °C, 40–80 °C, 50–80 °C and 50–120 °C. The energy densities in kWh/m^3 were calculated with the following equation:

$$\Delta E = Q \times \rho_s / 3600 \quad (2)$$

With ΔE the energy storage density in kWh/m^3, Q the heat of sorption (J/g dry composite) and ρ_s the bulk density of the dry composite (kg/m^3).

The heat of sorption is obtained by integrating the heat flow signal. As the experiments were carried out under a temperature change, corrections must be done to consider the heat required to heat the crucibles (from a blank test) and to heat the composite (c_p correction). The heat of sorption is thus calculated following the equation:

$$Q = (\Delta H_{exp} - \Delta H_{crucible} - mc_p \Delta T)/m \quad (3)$$

Where ΔH_{exp} is the integration of the heat flow signal during the test, $\Delta H_{crucible}$ is the integration of the heat flow signal during a blank test (empty crucibles), m is the anhydrous mass of composite, c_p is the heat capacity of the composite and ΔT is the difference of temperature of the sample during the test.

2.7. Multi-cycles stability test

The stability upon repeated adsorption/desorption steps was measured with the dynamic vapor sorption analyzer IGASorp from Hiden Isochema on the most promising material, i.e. SG/LiBr 53 wt%. Prior to the measurements, the sample was dried at 200 °C for 10 h. It was then hydrated at 30 °C and 29.5% RH (relative humidity) and dehydrated at 80 °C and 2.6% RH, both relative humidity corresponding to 12.5 mbar. This adsorption/desorption cycle was repeated, and the mass change was measured.

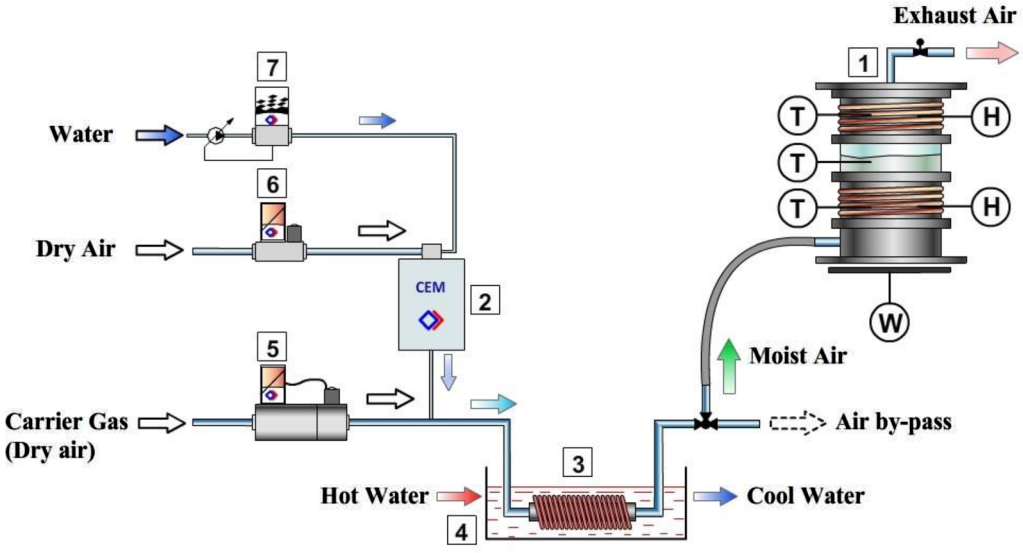

Fig. 1. Laboratory installation with open sorption reactor.

2.8. Water vapor sorption isotherms measurement

The water vapor sorption isotherms were measured for SG/LiBr 53 wt% with the dynamic vapor sorption analyzer IGASorp from Hiden Isochema. Prior to the measurements, the sample was dried at 200 °C for 10 h. The water vapor sorption isotherms were measured between 10 °C and 80 °C (temperature steps of 10 °C), with a RH step of 5% for temperatures between 10 °C and 30 °C and 3% for temperatures between 40 °C and 80 °C. After each isotherm, the sample was dried at 200 °C for 3 h.

2.9. Test on the laboratory open-type reactor

The hygrothermal behavior and energy performance characteristics during the adsorption step were studied in a laboratory open sorption reactor (packed bed) for the SG/LiBr 53 wt% composite. The experimental set up is shown on the Fig. 1. It is composed of the sorption reactor and the moist air handling system. The reactor is designed from three stacked cylindrical compartments, each holding a set of sensors.

The lower and upper reactor sections are identical. They perform the air conditioning function for the inlet and outlet air in order to avoid additional thermal losses and prevent water condensing on the inner reactor surface. Each section is equipped with one set of four standard K-type thermocouples and one HC2-P05 humidity probe from Rotronic. The middle section is transparent, wherein the material sample is hold by a thin metallic sieve. Four standard K-type thermocouples, which are placed in the middle section, measure the temperature in different locations of the material layer. The surface area for the air flow through the material is 0.05 m^2.

The online monitoring of the water mass adsorbed by the composite sample is provided by the high accuracy balance (Signum® Model 1 from Sartorius), whereon the reactor is mounted. The calibration of the balance was done in order to compensate the tubing connection and air static pressure in the reactor.

The moist air handling system includes the air humidification circuit, which is based on the Bronkhorst® vapor delivery solution (full range of air relative humidity), and the air heating circuit, which is designed with corrugated stainless steel coil flooded in the hot water bath (30–45 °C).

The accuracy characteristics of the used measuring devices and sensors are presented in Table 1.

The experimental method, to perform the adsorption step, consists of the following procedures:

(i) Drying the material sample in the laboratory oven at 150 °C for 12 h.
(ii) Preparation (pre-heating) of the installation for the test by running it at the targeted conditions at least 40 min prior to the test.
(iii) Cooling the material sample in the hermetic vessel to the room temperature and checking the residual water content using ~10 g in a moisture analyzer (model HE73 from Mettler Toledo).
(iv) Putting the material sample into the reactor and running the test in the targeted conditions. While the material is being layered inside the reactor, the air exits through the by-pass circuit.

The described method was applied to the material samples with masses between 200 and 245 g that represent a reactive layer of ~10 mm.

The used experimental conditions are shown in the Table 2.

The specific thermal power $\dot{Q}$ is calculated using the following relation:

$$\dot{Q} = \frac{\dot{m}_a C_{P,a}}{m} \Delta T_a \quad (4)$$

Here m is the mass of anhydrous material sample, $\dot{m}_a$ is the mass air flow rate through reactor (dry air), $C_{P,\,a}$ is the dry air heat capacity and ΔT_a is the temperature difference between inlet and outlet conditions.

3. Results and discussion

3.1. Synthesis and characterization of the four composite materials

Four composites were synthesized: two composites based on silica gel (SG) and two composites based on activated carbon (AC). The salt contents obtained by mass difference during the synthesis were 37 wt% and 53 wt% for the SG/LiBr composites and 32 wt% and 42 wt% for the AC/LiBr composites. Thanks to the multi-step incipient wetness protocol, the salt contents are high, compared to the reported LiBr-based composites [33,40,67,68].

The salt content of SG/LiBr composites obtained by XRF are in fair agreement with those obtained by mass difference during the synthesis: 32.5 wt% instead of 37 wt% and 53.7 wt% instead of 53 wt%. Using ICP, the SG/LiBr are found to contain 36.5 and 55.8 wt% LiBr. For the AC/LiBr composites, the salt contents obtained by TGA measurements were in fair agreement with those obtained by mass difference during the synthesis: 28.5 wt% and 42.5 wt% instead of 32 wt% and 42 wt% respectively.

The X-ray diffraction measurements were performed in order to identify the crystalline form of LiBr in the different composites. For hydrated samples, the X-ray signal corresponds to a purely amorphous material, for all the composites (not shown). This is explained by the dissolution of LiBr in ambient moisture. For dried composites, the X-ray diffraction patterns are presented in Fig. 2.

Concerning the SG/LiBr composites, the pores size is large enough to allow the formation of LiBr crystals sufficiently large to be indexed by XRD. Two allotropic forms of LiBr are observed. For the AC/LiBr composites, the observation of LiBr crystals is more difficult due to the small pores size of the activated carbon (microporous material). The anhydrous LiBr is still observed despite this microporosity of the activated carbon for AC/LiBr 42 wt% (Fig. 2c), and this could indicate the presence of LiBr crystals outside of the particles (on the surface). This means that AC is not able to contain such a high LiBr content in its porosity and that such high salt amounts should be avoided for AC.

The homogeneity of the salt dispersion inside the composites was evaluated by SEM-EDX. The SG/LiBr composites presented a good homogeneity of the impregnation (Fig. 3), the Br is well observed wherever in the particle. Slight diffusion inside the resin is observed, but it does not prevent to observe a strong Br signal at the center of the particles.

For AC/LiBr composites, mappings on entire particles cannot be acquired due to shading effects in the SEM room. This is due to the big size of the particles, making it necessary to map with a low magnification. Mappings were thus acquired on corners of particles, which does not prevent from comparing central and outer areas. The results are presented in Fig. 4. For AC/LiBr 32 wt%, the Br area corresponds to the particle perimeter and there is no visible difference between central and outer areas, suggesting a good quality of impregnation for this sample. For AC/LiBr 42 wt%, marked differences inside the particles were

Table 1
Accuracy characteristics of the measuring devices and sensors for full scale range used in the lab-scale prototype.

Nomenclature	Accuracy
Air flow meter Bronkhorst® IN-FLOW F-203AV	± 0.1%
Air flow meter Bronkhorst® IN-FLOW F-201AV	± 0.1%
Water flow meter Bronkhorst® miniCORI-FLOW M-13	± 0.5 g/h
Air humidity and temperature sensor Rotronic HC2-P05	± 1.5% R.H., ± 0.3 °C
K-type standard thermocouple	± 0.4%
Balance Sartorius Signum® Model 1	± 0.5 g
Moisture analyzer Mettler Toledo HE73	± 1.0 mg

Table 2
Experimental conditions for composite material SG/LiBr 53 wt% used in the laboratory open sorption reactor.

Anhydrous sample mass (g)	224
Initial water mass uptake (g/g)	3.4×10^{-3}
Dry air volume flow rate (l/min)	215
Average inlet air temperature (°C)	28.7
Average inlet water vapor pressure (Pa)	1248

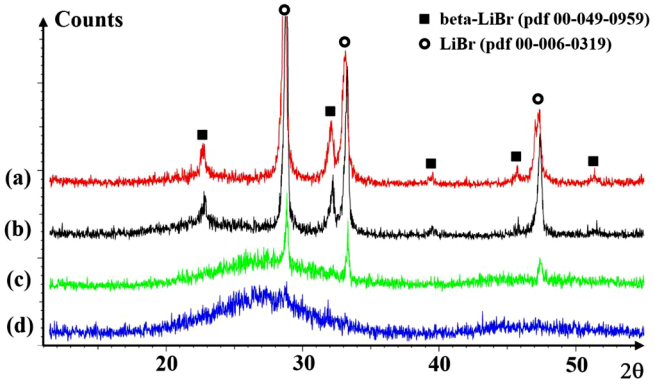

Fig. 2. X-ray diffraction patterns of SG/LiBr and AC/LiBr composites:(a) SG/LiBr 53 wt%; (b) SG/LiBr 37 wt%; (c) AC/LiBr 42 wt%; (d) AC/LiBr 32 wt%.

observed, with some outer areas nearly exclusively composed on LiBr (in blue). Together with XRD data that show crystallization of LiBr despite the very low pore diameter of AC, this is compatible with partial crystallization on the surface of the particles. Compared with SG, this result indicates that AC is closer from saturation in LiBr than SG during the impregnation. It is less prone to migrate towards the center of the particles. The presence of salt on the surface of the composite could lead to instability issues for this composite.

Concerning the structural characteristics of the LiBr-based composites, obtained from the nitrogen sorption measurement at −196 °C (Table 3), both specific surface area and total pore volume values decrease with the incorporation of LiBr into the matrix, which indicates that the salt is located in the pores of the host matrix. Considering the total pore volumes of the matrix and of the composite, the salt content SC_{BET} can be calculated thanks to Eq. (3), assuming that the salt occupies the difference of volume between the matrix and the composite [32,43]:

$$SC_{BET} = \frac{V_{P_{matrix}} - V_{P_{composite}}}{V_{P_{matrix}} + \frac{1}{\rho_{salt}}} \quad (5)$$

With V_p the total pore volume (cm^3/g) and ρ_{salt} the density of LiBr (3.46 g/cm^3 or 3460 kg/m^3).

According to this equation, the salt content calculated from the total pore volumes are in fair agreement with the salt content obtained by mass difference during the synthesis for SG/LiBr 53 wt% and AC/LiBr 32 wt%, for which the calculated salt contents are 55 wt% and 33 wt% respectively. For the two other composites, small differences were observed between the calculated salt contents and the one obtained by mass difference during the synthesis. For SG/LiBr 37 wt%, the calculated SC_{BET} is 32 wt%, this is also different from the salt content measured by XRF (42 wt%). This heterogeneity of the salt content may be explained by a heterogeneity of the salt dispersion from grain to grain, which means that some grains are more filled with LiBr, whereas other are less filled by the salt. This heterogeneity is corrected with the second impregnation step, leading to SG/LiBr 53 wt%. For the AC/LiBr 42 wt%, the calculated salt content is 35 wt%, whereas the salt content measured by thermal analysis was 42.5 wt%, very close to the salt content obtained by mass difference during the synthesis. For this composite, the difference of salt contents could be explained by the presence of salt on the surface of the grains, as it was observed by SEM.

The comparison of the pore size distributions (pores radius r_p) of the SG/LiBr composites and the silica gel (Fig. 5), obtained by the BJH treatment of the desorption branch of the nitrogen sorption isotherm, shows that during the impregnation, the salt filled the pores homogeneously. On the contrary of what was observed for SG/$CaCl_2$ and SG/$SrBr_2$ composites [32,43], the smallest pores are not completely filled

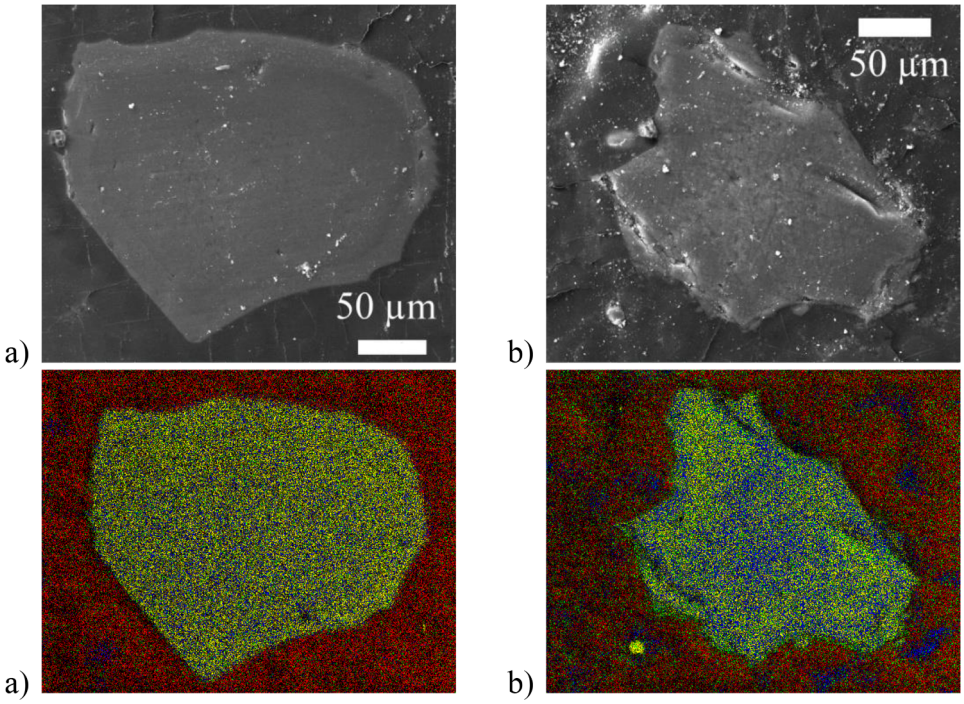

Fig. 3. Cross-section SEM micrograph and mapping of SG/LiBr composites: a) SG/LiBr 37 wt%, b) SG/LiBr 53 wt% composite. C is in red, Br in blue and Si in yellow. (For interpretation of the references to color in this figure legend, the reader is referred to the web version of this article.)

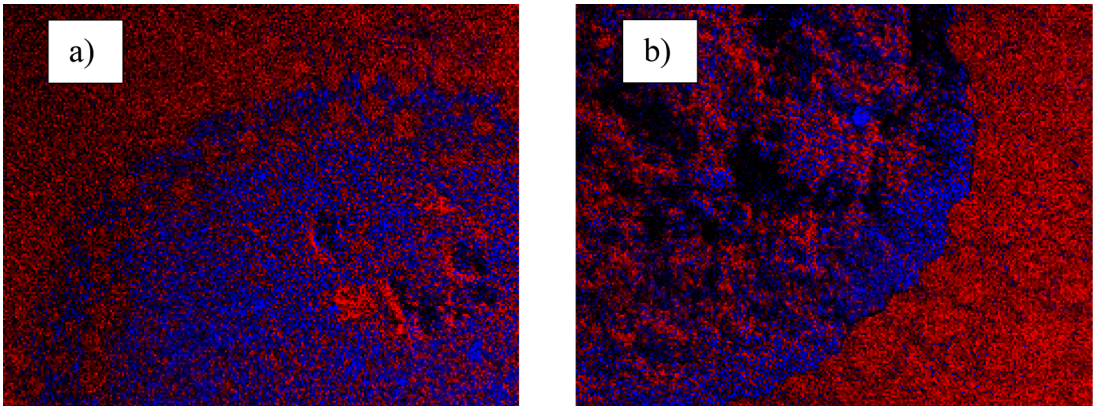

Fig. 4. Cross-section SEM micrograph and mapping of AC/LiBr composites: a) AC/LiBr 32 wt%, b) AC/LiBr 42 wt% composite. C is in red and Br in blue. (For interpretation of the references to color in this figure legend, the reader is referred to the web version of this article.)

Table 3
Structural characteristics of silica gel, SG/LiBr composites, activated carbon and AC/LiBr composites obtained from BET analysis of the nitrogen sorption isotherm at −196 °C.

	Specific surface area (m^2/g)	Total pore volume (cm^3/g)	Average pore diameter (nm)
SG	372	0.89	10
SG/LiBr 37 wt%	188	0.51	11
SG/LiBr 53 wt%	87	0.24	11
AC	1282	0.67	2
AC/LiBr 32 wt%	589	0.36	2
AC/LiBr 42 wt%	544	0.33	2

during the impregnation process. All the pores are filled partially, which lets a free porosity for the access of water. The same observations can be made for the AC/LiBr composites with the MP-plot treatment (giving the pores diameter d_p) of the desorption branch of the nitrogen sorption isotherm at −196 °C (Fig. 6). The salt filled partially all the pores without completely filling the smallest ones.

The energy storage densities were measured at different temperature conditions representative of the application ones. Results are shown on Fig. 7.

Firstly, Fig. 7 highlights that the SG/LiBr 53 wt% has the highest energy storage densities compared to the three others. In conditions representative of space heating applications, this composite exhibits high energy storage densities of 261 kWh/m^3 (30–80 °C range, at 12.5 mbar) and 381 kWh/m^3 (30–120 °C, 12.5 mbar). The energy storage densities of this SG/LiBr 53 wt% composite remain particularly high when the adsorption temperature increases, as it is the case for hot water production applications, with values of 181 kWh/m^3 (40–80 °C, 12.5 mbar) and 131 kWh/m^3 in the worse scenario (50–80 °C, 12.5 mbar). The performance of this composite outperforms all the previously reported water sorbents. This composite is particularly promising for thermal heat storage for space heating and hot water production applications.

The performances of the composite SG/LiBr 37 wt% are much lower than the one at 53 wt%, agreeing with the fact that the energy storage density depends on the salt content. Nevertheless, the difference of salt content alone cannot explain the difference of energy storage densities. A difference of sorption heats and of bulk densities of both composites can also influence the energy storage densities. Between 30–80 °C at 12.5 mbar, the energy storage density of SG/LiBr 37 wt% is 119 kWh/m^3, which is quite low for the space heating applications, and it becomes lower than 100 kWh/m^3 when increasing the adsorption temperature. The same comments can be done for the composite AC/LiBr 32 wt% whose energy storage density is 131 kWh/m^3 between 30 and 80 °C at 12.5 mbar but becomes lower than 100 kWh/m^3 when increasing the adsorption temperature. The composite AC/LiBr 42 wt% has an interesting energy storage density of 186 kWh/m^3 between 30 and 80 °C at 12.5 mbar and 223 kWh/m^3 when increasing the desorption temperature to 120 °C. The energy storage density remains higher than 100 kWh/m^3 between 40 and 80 °C at 12.5 mbar (125 kWh/m^3) but is only 75 kWh/m^3 between 50 and 80 °C at 12.5 mbar. For this last composite, the visual observation of the sample after the efficiency tests shows that the particles of composite became whiter. It indicates that the salt may have leaked out from the pores and has recrystallized at the surface of the grains. This shows an instability of this composite, which confirms the results from the SEM observations and the X-ray diffraction data and explains why this composite is not usable for the thermal heat storage for space heating and hot water production applications.

The isobars at 12.5 mbar for the four composites are presented in Fig. 8. Unsurprisingly, the composite SG/LiBr 53 wt% obtained the highest mass uptakes, higher than 0.6 g/g at 30 °C. The most interesting in this graph is that for the SG-based composites and for AC/LiBr 32 wt %, the totality of the sorbed water is removed at 120 °C, which confirmed the possibility of using solar collectors to completely dry these composites. Surprisingly, the mass uptake at 120 °C of AC/LiBr 42 wt%

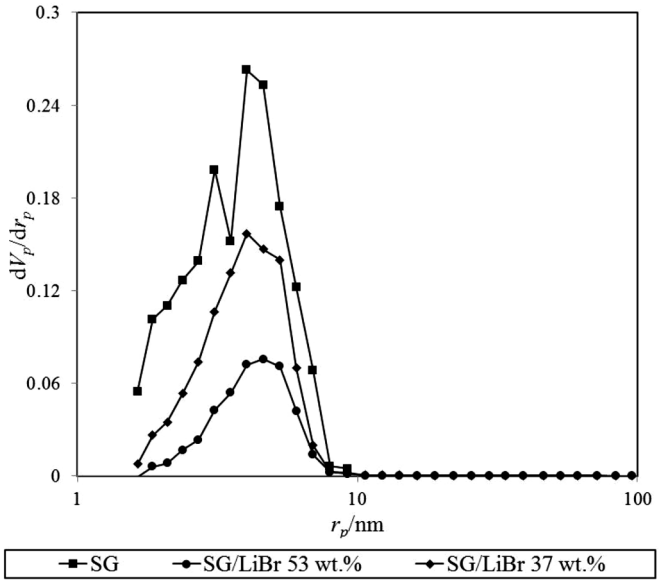

Fig. 5. Pore size distribution obtained by BJH treatment of the desorption branch of the nitrogen sorption isotherm at −196 °C for silica gel SG, and both SG/LiBr composites 37 wt% and 53 wt%, with V_p the pore volume and r_p the pores radius.

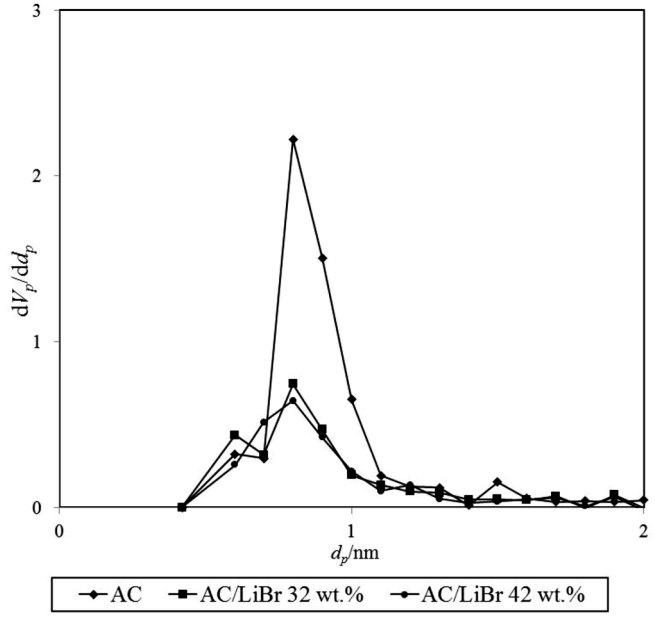

Fig. 6. Pore size distribution obtained by the MP-plot treatment of the desorption branch of the nitrogen sorption isotherm at −196 °C for activated carbon AC, and both AC/LiBr composites 32 wt% and 42 wt%, with V_p the pore volume and d_p the pore diameter.

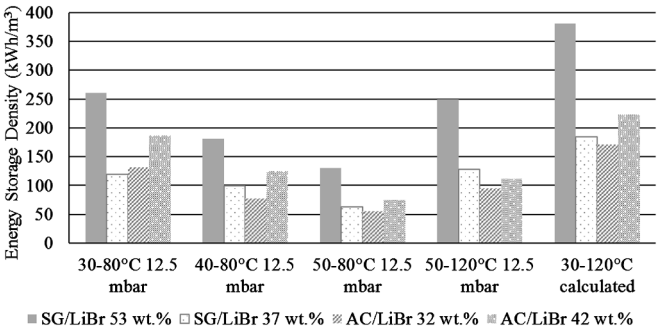

Fig. 7. Comparison of the energy storage densities of the four composites at different temperature conditions.

remains high (around 0.2 g/g), which may be due to the instability issues described earlier.

Based on these results of the efficiency tests, it was decided to pursue the study on the SG/LiBr 53 wt% which exhibits the highest energy storage densities.

3.2. Sorption properties of SG/LiBr 53 wt%

The composite SG/LiBr 53 wt% was submitted to the multi-cycles stability tests. The results are presented in Fig. 9, representing the mass uptake (at the equilibrium) at 30 °C and at 80 °C, both steps at 12.5 mbar for the different successive cycles. This composite SG/LiBr 53 wt% exhibits a very high stability upon 10 adsorption/desorption cycles, which is very promising for the thermal heat storage applications, which requires the use of the storage materials during at least 25 years (i.e. requires high stability and reproducibility of the performances for at least 25 cycles).

The water sorption isotherms were measured between 10 °C and 80 °C (Fig. 10). The water vapor sorption is high even at low water pressure. On the contrary of the results of Gordeeva et al. [47] and Tanashev et al. [70] on mesoporous silica gel and LiBr composites, the crystalline monohydrate LiBr is not observed in these isotherms. Indeed, the LiBr.H_2O state corresponds to a mass uptake of 0.11 g H_2O/g composite, and this mass uptake is rapidly overpassed at low water pressure. The shape of the isotherms shows that the water vapor sorption mechanism is mainly due to the absorption by the LiBr solution, which is rapidly formed in the pores of silica gel. This rapid formation of salt solution in the matrix pores could have led to instability due to a possible salt leakage, but the multi-cycles stability test has demonstrated that the silica gel is a stabilizing environment for LiBr, even when the salt is in solution in the matrix pores. The high mass uptake at low vapor pressure is also interesting for the applications.

Table 4 shows the comparison of the adsorption properties of SG/LiBr 53 wt% and other LiBr based composites from literature. As can be seen in Table 4, the SG/LiBr 53 wt% outperforms the other LiBr based composites described in the literature. Even compared with SG/LiBr 57 wt%, which contains more LiBr, the water mass uptake at 40 °C and 13 mbar is much higher for the composite SG/LiBr 53 wt% (0.48 g/g vs. 0.29 g/g).

Fig. 11 represents the characteristic curve (mass uptake vs. adsorption potential) based on the Polanyi theory of the pore filling mechanism [72,73]. The adsorption potential A is expressed as follows:

$$A = RTLn\left(\frac{P_s}{P}\right) \quad (6)$$

With R the gas constant (J/mol.K), T the temperature (K), P_s the saturation vapor pressure (Pa) and P the water vapor pressure (Pa).

The Dubinin-Astakhov (DA) model [74] can be used to fit the experimental data. The DA model is expressed as follows:

$$w = w_0 exp\left[-\left(\frac{A}{E}\right)^n\right] \quad (7)$$

With w the adsorbed volume or the mass uptake (when the density is taken equal to 1 g/cm^3, as it is the case here), and E the characteristic energy of adsorption.

The parameters of the DA model are presented in Table 5.

The comparison between the experimental data and the calculated data obtained by the DA model for the water sorption isotherms of SG/LiBr 53 wt% (Fig. 12) confirms the ability of the DA model to well represent the experimental mass uptakes. This model can be used in future system's simulations to calculate the mass uptake at the equilibrium depending on the temperature and pressure conditions.

The isosteric heat of sorption ΔH_{is} can be calculated for different mass uptakes thanks to the Clapeyron diagram representing Ln(P) vs −1/T (Fig. 13 and Table 6). The isosteric heat of sorption decreases with the increasing mass uptake. It is equal to 56.5 kJ/mol at a water uptake of 0.2 g/g. This value is higher than the one reported for SWS-2C (44.7 kJ/mol for $N > 2$ mol/mol) [33] and the one reported for SiO_2/LiBr by sol-gel process (40.5 kJ/mol for water uptake > 0.06 g/g) [69]. The isosteric heat of sorption remains high at high water uptake, with a minimum value of 45.2 kJ/mol. These values are in fair agreement with the experimental calorimetric measurements, for which an average value of 2630 J/g H_2O or 47.3 kJ/mol H_2O was obtained.

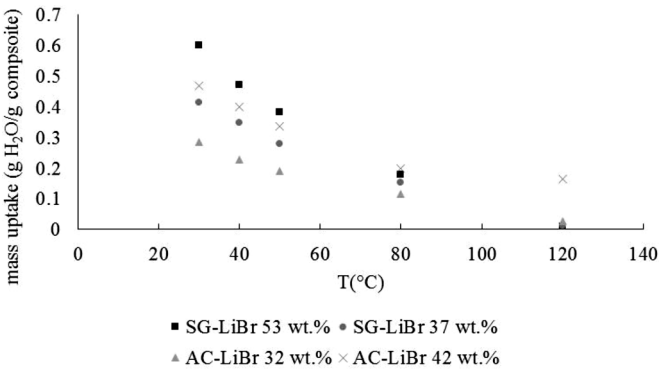

Fig. 8. Comparison of the isobar at 12.5 mbar for the four composites.

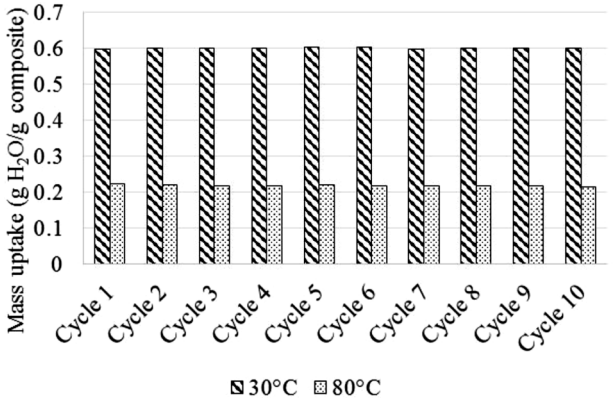

Fig. 9. Comparison of the mass uptakes at 30 °C and 80 °C at 12.5 mbar upon successive adsorption/desorption cycles.

A polynomial model (Eq. (8)) represents the dependence of the isosteric heat of sorption (in J/g) on the water uptake w.

$$\Delta H_{is}\ (J/g) = -1257.5w^3 + 3824.9w^2 - 3774.7w + 3733.8 \quad (8)$$

3.3. Results of the adsorption test of SG/LiBr 53 wt% in the open sorption set-up

The adsorption step test was performed for 224 g of SG/LiBr 53 wt% composite material in the laboratory set-up (see Fig. 1). The hygrothermal behavior of this material is shown on the Fig. 14 (a, b and c). The generation of the specific thermal power $\dot{Q}$, related to the time t or to the water uptake w, is shown on the Fig. 15 (a and b). The outlet temperature (see Fig. 14a, the curve "outlet condition") represents the average temperature measured by four K-type thermocouples situated just above the sample surface at the distance being not higher than ~10 mm. This approach gives a reliable image of the air temperature at the sample outlet, because the thermal losses are negligible at that location of measurement.

Although the equilibrium water mass uptake, calculated from the experimental inlet conditions in Table 1, supposed to be 0.63 g/g, the final experimental water mass uptake was measured as high as 0.33 g/g (see Fig. 14c). The same final water mass uptake was confirmed with the moisture analyzer HE73. The adsorption test lasted 3 h 26 min, whereas the outlet temperature has reached the stable level (~31 °C) in 1 h 24 min (see Fig. 14a). The outlet water vapor pressure is delayed in comparison with outlet temperature and it has reached its stable level of ~11.5 mbar in 1 h 53 min. However, even if the monitored temperature and water vapor pressure remained stable at least during 2 h,

Table 4
Comparison of adsorption properties of SG/LiBr 53 wt% and other LiBr based composites from literature.

Composite	Ref	T (°C)	P (mbar)	w (g/g)	w (g/g) SG/LiBr 53 wt%
AC/LiBr 8.5%	[68]	30	25	0.1	0.83 (21 mbar)
Alumina/LiBr 13.2%	[68]	30	25	0.3	0.83 (21 mbar)
SG/LiBr 57%	[47,70]	40	13	0.29	0.48
AC/LiBr 29%	[33]	40	13	0.22	0.48
		80	13	0.116	0.19
		40–80	13	0.104	0.29
Expanded Graphite/LiBr 33%	[33]	40	13	0.24	0.48
		80	13	0.068	0.19
		40–80	13	0.172	0.29

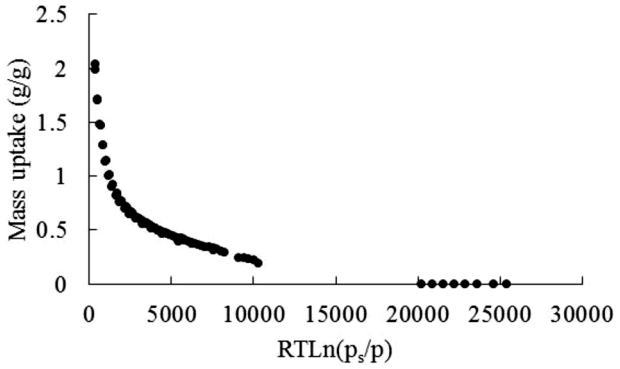

Fig. 11. Characteristic curve of the water vapor sorption on SG/LiBr 53 wt%.

Table 5
Parameters of the DA model fitting the water sorption equilibrium data of SG/LiBr 53 wt%.

n	0.2
w_0 (g/g)	15.86
E (J/mol)	8.175

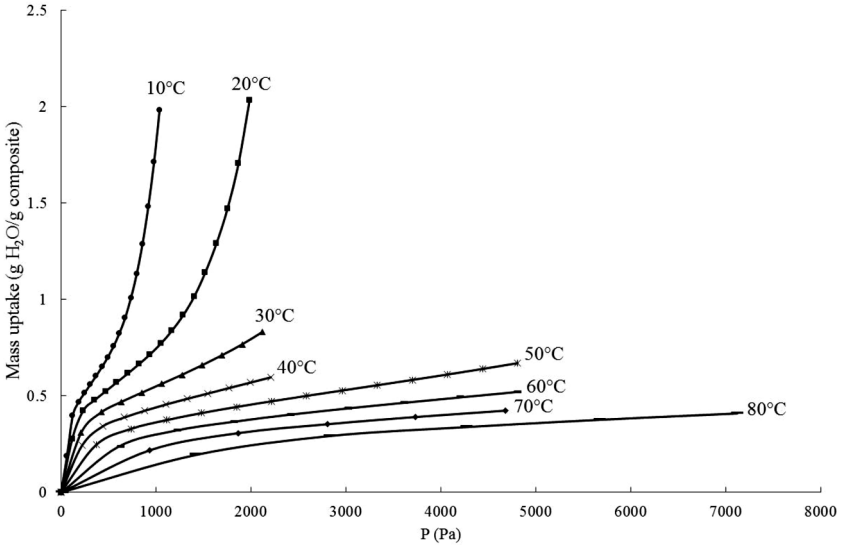

Fig. 10. Water vapor sorption isotherms of SG/LiBr 53 wt%.

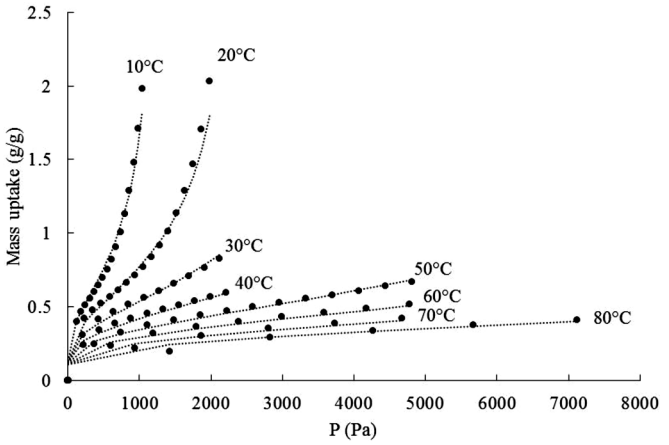

Fig. 12. Comparison between the experimental data (points) and calculated data by the DA model (dotted line) for the water vapor sorption isotherms of SG/LiBr 53 wt%.

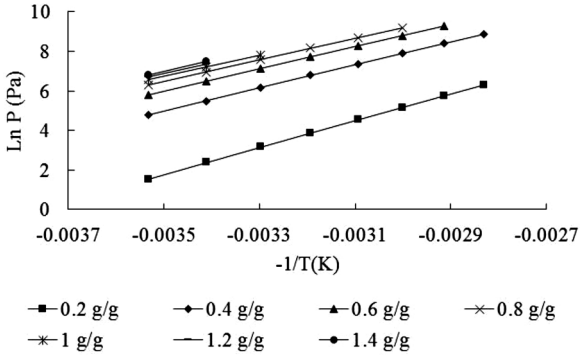

Fig. 13. Clapeyron diagram Ln(P) vs. −1/T for the water sorption of SG/LiBr 53 wt%.

Table 6
Isosteric heat of sorption of SG/LiBr 53 wt% at different water equilibrium uptakes.

Equilibrium mass uptake (g/g)	ΔH_{is} (J/g H_2O)	ΔH_{is} (kJ/mol H_2O)
0.2	3137	56.5
0.4	2717	48.9
0.6	2590	46.6
0.8	2537	45.7
1	2532	45.6
1.2	2508	45.2
1.4	2508	45.2

the adsorption reaction was still going on, as follows from the water mass signal (see Fig. 14c), but it had not any significant thermal effect (see Fig. 15a). The water uptake profile presents a distinct “knee” around 1 h 12 min (see Fig. 14c). Therefore, the adsorption test is composed of two steps:

(i) intensive thermal power generation process, that is characterized by the water mass uptakes up to 0.22 - 0.25 g/g and specific thermal powers between 40 and 286 W/kg (see Figs. 14c and 15b);
(ii) slow thermal power generation process, for which the water mass uptake overcomes the threshold of 0.22–0.25 g/g and the specific thermal power is found to be as low as 40 W/kg.

Such a behavior is related to the specific sorption mechanism and the used experimental conditions, and it can be corrected by a variable air flow rate or a controlled air humidification. The high equilibrium

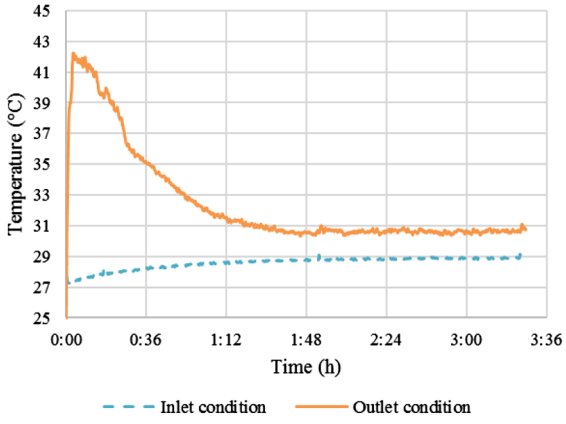

(a) Temperature profile at the inlet and outlet of material sample.

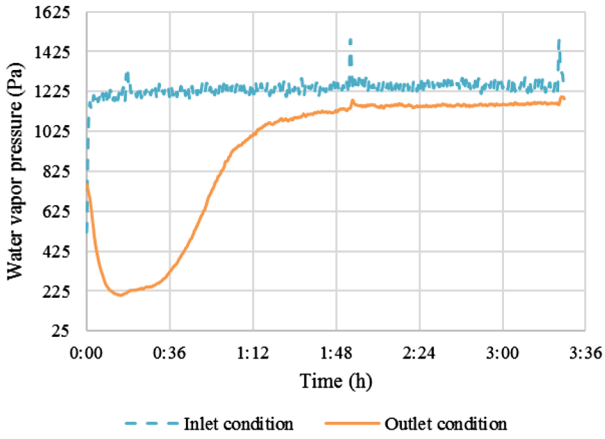

(b) Water vapor profile at the inlet and outlet of material sample.

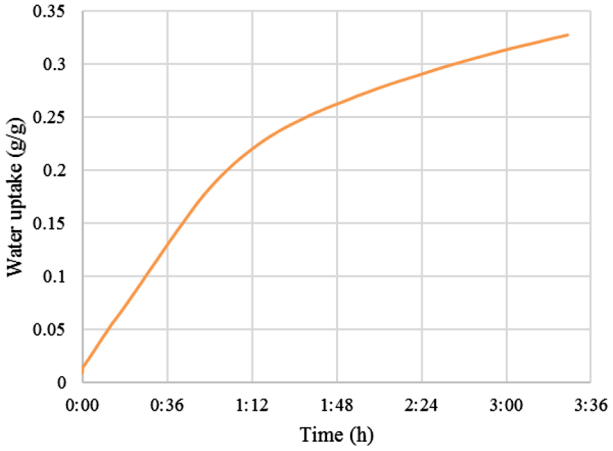

(c) Evolution of water uptake profile inside the material sample.

Fig. 14. Hygrothermal behavior of 224 g of SG/LiBr 53 wt% composite material for 28.7 °C as average inlet air temperature and 1248 Pa as reference water vapor pressure.

water uptake set by the air conditions at the reactor inlet (see Fig. 10) results in the initially fast water vapor sorption mechanism and the specific thermal power reaches the maximum of 286 W/kg in less than 1 min. Since the solid is heated very quickly, without being effectively cooled down by the incoming air, the adsorption potential A dynamically swings in the range between 3.4 and 6.3 kJ/mol. This swing

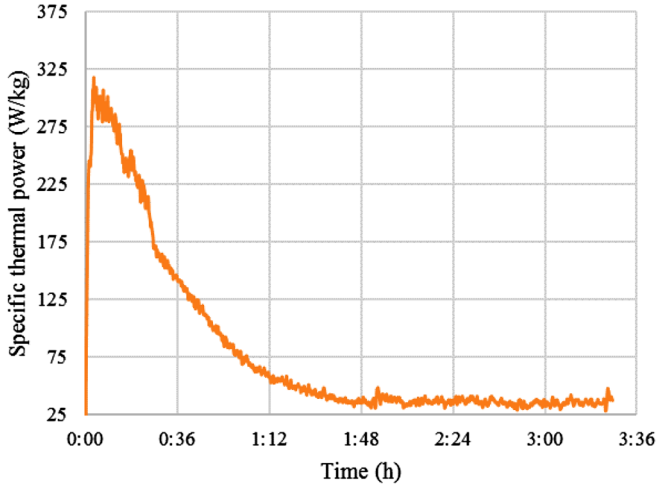

(a) Specific thermal power vs. time.

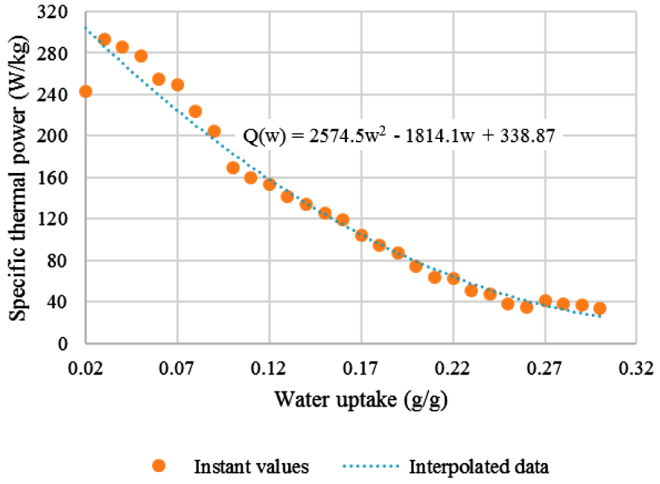

(b) Specific thermal power vs. water uptake.

Fig. 15. Specific thermal power recorded for SG/LiBr 53 wt% composite material for 28.7 °C as average inlet air temperature and 1248 Pa as reference water vapor pressure.

occurs on the time span between ~12 min and ~1 h 12 min, considering the outlet air temperature (see Fig. 14a) and the average water vapor pressure between inlet and outlet conditions in Fig. 14b for the calculation of adsorption potential with formula (4). The dynamic changes of adsorption potential cause the equilibrium water mass uptake to vary also dynamically from 0.36 g/g to 0.56 g/g (see Fig. 11) on the same time span (see Fig. 14). First, the equilibrium mass uptake drops down to 0.36 g/g as soon as the temperature and the thermal power reach the peak values, provoking the sharp decrease in the heat generation phenomenon that can be observed at ~27 min in Figs. 14a and 15a. Afterwards, the adsorption potential springs back to 3.4 kJ/mol (due to the solid cooling) and the equilibrium mass uptake resets to 0.56 g/g after ~1 h 12 min, whereas the characteristic "knee" becomes visible (see Fig. 14c). The further sorption phenomenon occurs at somewhat higher temperature of ~31 °C with the slower kinetic rate (see Fig. 14a, c). Moreover, during the fast sorption stage between ~12 min and ~1 h 12 min, the sample mass rises also fast, creating the heavily hydrated layer with additional flow resistance for the inlet air. At the same time, the hydrated particles start to be agglomerated, which results in the formation of the preferential air passages through the material layer. The sorption process becomes non-homogeneous through the material and the thermal power attenuates.

The analysis of hygrothermal behavior in the open sorption reactor leads to the conclusion that the hydration process has to be controlled by a special air distribution/conditioning device, in order to take into account the described above issues. In case of the uncontrolled sorption behavior, as shown on the Figs. 14 and 15, the power generation process is only effective up to 0.22 - 0.25 g/g of water mass uptake. The specific thermal power in this region of water uptakes varies between 40 and 286 W/kg.

The instant values of the specific thermal power from the Fig. 15b can be approximated by the following polynomial expression:

$$\dot{Q}(w) = 2574.5w^2 - 1814.1w + 338.87 \quad (9)$$

The discharging energy storage density at the material level in the applied experimental conditions can be evaluated using the following equation:

$$\Delta E = \rho_s \int_0^{t_e} \dot{Q}(t)\mathrm{d}t \quad (10)$$

Here ρ_s is the density of the material, which for the bulk fraction is equal to 847.8 kg/m^3 and t_e is the upper integration time limit. Therefore, the sample of SG/LiBr 53 wt% composite material has achieved 232 kWh/m^3 of energy storage density during 3 h 26 min of adsorption test, that corresponds to 0.33 g/g of final water mass uptake. At the same time, the tested sample has reached already 160 kWh/m^3 during the first 1 h 12 min before the water uptake has overcome the threshold of 0.22 g/g.

4. Conclusion

Four composites based on LiBr and two different porous matrices (silica gel and activated carbon) were synthesized with the multi-step wetness impregnation process, which enables to reach high salt contents between 32 and 53 wt%. The incorporated salt was well dispersed inside the silica gel pores except only for the AC/LiBr 42 wt% that shows salt crystals on the surface of the activated carbon. The efficiency performances of these composites were compared at different temperature conditions, representative of the heat storage for space heating and hot water production applications. The SG/LiBr 53 wt% composite presents the most promising performances compared to the three others and to the previously reported composites, with an energy storage density of 261 kWh/m^3 ($T_{adsorption}$ = 30 °C, $T_{desorption}$ = 80 °C and 12.5 mbar) and 381 kWh/m^3 when the desorption temperature is increased to 120 °C. These values are representative of the sorption equilibrium and are measured at the 50 mg scale.

Based on these results, this SG/LiBr 53 wt% composite was further tested, by measuring the water sorption isotherms between 10 °C and 80 °C. It showed a very good multi-cycles stability upon 10 adsorption/desorption cycles. The water vapor sorption isotherms were fitted with a Dubinin–Astakhov model. The isosteric heats of sorption were determined for several mass uptakes. This SG/LiBr 53 wt% composite was tested in an adsorption step in a laboratory open-type reactor at a higher scale. A specific heat power up to 286 W/kg was obtained with a mass uptake of 0.22–0.25 g/g, which corresponds to an energy storage density of 160–175 kWh/m^3. In these practical conditions, the material does not reach the sorption equilibrium.

All these characterization tests confirmed the promising behavior of SG/LiBr 53 wt% used for water sorption for heat storage for residential heating and hot water production applications.

CRediT authorship contribution statement

Emilie Courbon: Investigation, Methodology, Writing - original draft, Writing - review & editing, Validation, Formal analysis. **Pierre D'Ans:** Investigation, Methodology, Writing - original draft, Writing - review & editing, Validation. **Oleksandr Skrylnyk:** Investigation, Methodology, Writing - original draft, Writing - review & editing,

Validation, Formal analysis. **Marc Frère:** Project administration, Supervision, Validation.

Declaration of Competing Interest

The authors declare that they have no known competing financial interests or personal relationships that could have appeared to influence the work reported in this paper.

Acknowledgments

The authors gratefully acknowledge the Walloon Region and the European Union for funding the STOCC project, in the frame of FEDER program 2014–2020 (Fond Européen de Développement Régional), under the project reference FEDER C3E2D-STOCC.

References

[1] G. Li, Organic Rankine cycle performance evaluation and thermoeconomic assessment with various applications part I: energy and exergy performance evaluation, Renew. Sustain. Energy Rev. 53 (2016) 477–499, https://doi.org/10.1016/j.rser.2015.08.066.
[2] G. Li, X. Zheng, Thermal energy storage system integration forms for a sustainable future, Renew. Sustain. Energy Rev. 62 (2016) 736–757, https://doi.org/10.1016/j.rser.2016.04.076.
[3] G. Li, Energy and exergy performance assessments for latent heat thermal energy storage systems, Renew. Sustain. Energy Rev. 51 (2015) 926–954, https://doi.org/10.1016/j.rser.2015.06.052.
[4] G. Li, Y. Hwang, R. Radermacher, H.H. Chun, Review of cold storage materials for subzero applications, Energy 51 (2013) 1–17, https://doi.org/10.1016/j.energy.2012.12.002.
[5] G. Li, Y. Hwang, R. Radermacher, Review of cold storage materials for air conditioning application, Int. J. Refrig. 35 (2012) 2053–2077, https://doi.org/10.1016/j.ijrefrig.2012.06.003.
[6] G. Li, Y. Hwang, Energy storage systems for buildings, in: J.E. Gonzalez, M. Krarti (Eds.), Handbook of Integrated and
Sustainable Buildings. Equipment and Systems: Volume I: Energy Systems, ASME Press, 2017, , https://doi.org/10.1115/1.861271_ch8.
[7] D. Aydin, S.P. Casey, S. Riffat, The latest advancements on thermochemical heat storage systems, Renew. Sustain. Energy Rev. 41 (2015) 356–367, https://doi.org/10.1016/j.rser.2014.08.054.
[8] L.F. Cabeza, A. Solé, C. Barreneche, Review on sorption materials and technologies for heat pumps and thermal energy storage, Renew. Energy 110 (2017) 3–39, https://doi.org/10.1016/j.renene.2016.09.059.
[9] K.E. N'Tsoukpoe, H. Liu, N. Le Pierr??s, L. Luo, A review on long-term sorption solar energy storage, Renew. Sustain. Energy Rev. 13 (2009) 2385–2396, https://doi.org/10.1016/j.rser.2009.05.008.
[10] D. Lefebvre, F.H. Tezel, A review of energy storage technologies with a focus on adsorption thermal energy storage processes for heating applications, Renew. Sustain. Energy Rev. 67 (2017) 116–125, https://doi.org/10.1016/j.rser.2016.08.019.
[11] A. Solé, I. Martorell, L.F. Cabeza, State of the art on gas-solid thermochemical energy storage systems and reactors for building applications, Renew. Sustain. Energy Rev. 47 (2015) 386–398, https://doi.org/10.1016/j.rser.2015.03.077.
[12] M. Aneke, M. Wang, Energy storage technologies and real life applications – a state of the art review, Appl. Energy 179 (2016) 350–377, https://doi.org/10.1016/j.apenergy.2016.06.097.
[13] G. Li, S. Qian, H. Lee, Y. Hwang, R. Radermacher, Experimental investigation of energy and exergy performance of short term adsorption heat storage for residential application, Energy 65 (2014) 675–691, https://doi.org/10.1016/j.energy.2013.12.017.
[14] G. Li, Y. Hwang, R. Radermacher, Experimental investigation on energy and exergy performance of adsorption cold storage for space cooling application, Int. J. Refrig. 44 (2014) 23–35, https://doi.org/10.1016/j.ijrefrig.2014.05.013.
[15] F. Kuznik, K. Johannes, C. Obrecht, D. David, A review on recent developments in physisorption thermal energy storage for building applications, Renew. Sustain. Energy Rev. 94 (2018) 576–586, https://doi.org/10.1016/j.rser.2018.06.038.
[16] P. Tatsidjodoung, N. Le Pierrès, L. Luo, A review of potential materials for thermal energy storage in building applications, Renew. Sustain. Energy Rev. 18 (2013) 327–349, https://doi.org/10.1016/j.rser.2012.10.025.
[17] D. Dicaire, F.H. Tezel, Regeneration and efficiency characterization of hybrid adsorbent for thermal energy storage of excess and solar heat, Renew. Energy 36 (2011) 986–992, https://doi.org/10.1016/j.renene.2010.08.031.
[18] T. Yan, R.Z. Wang, T.X. Li, L.W. Wang, I.T. Fred, A review of promising candidate reactions for chemical heat storage, Renew. Sustain. Energy Rev. 43 (2015) 13–31, https://doi.org/10.1016/j.rser.2014.11.015.
[19] H. Deshmukh, M.P. Maiya, S. Srinivasa Murthy, Study of sorption based energy storage system with silica gel for heating application, Appl. Therm. Eng. 111 (2017) 1640–1646, https://doi.org/10.1016/j.applthermaleng.2016.07.069.
[20] K. Lim, J. Che, J. Lee, Experimental study on adsorption characteristics of a water and silica-gel based thermal energy storage (TES) system, Appl. Therm. Eng. 110 (2017) 80–88, https://doi.org/10.1016/j.applthermaleng.2016.08.098.
[21] L. Rustam, F. Jeremias, S.K. Henninger, T. Wolff, G.M. Munz, Tuning of adsorbent properties – oxidative hydrophilization of activated carbon monoliths for heat storage applications, Energy Build. 196 (2019) 206–213, https://doi.org/10.1016/j.enbuild.2019.05.024.
[22] R. Köll, W. van Helden, G. Engel, W. Wagner, B. Dang, J. Jänchen, H. Kerskes, T. Badenhop, T. Herzog, An experimental investigation of a realistic-scale seasonal solar adsorption storage system for buildings, Sol. Energy 155 (2017) 388–397, https://doi.org/10.1016/j.solener.2017.06.043.
[23] S.K. Henninger, S.J. Ernst, L. Gordeeva, P. Bendix, D. Fröhlich, A.D. Grekova, L. Bonaccorsi, Y. Aristov, J. Jaenchen, New materials for adsorption heat transformation and storage, Renew. Energy 110 (2017) 59–68, https://doi.org/10.1016/j.renene.2016.08.041.
[24] A. Permyakova, O. Skrylnyk, E. Courbon, M. Affram, S. Wang, U.-.H. Lee, A.H. Valekar, F. Nouar, G. Mouchaham, T. Devic, G. De Weireld, J.-.S. Chang, N. Steunou, M. Frère, C. Serre, Synthesis optimization, shaping and heat reallocation evaluation of the hydrophilic metal organic framework MIL-160(Al), ChemSusChem (2017), https://doi.org/10.1002/cssc.201700164.
[25] A. Elsayed, E. Elsayed, R. AL-Dadah, S. Mahmoud, A. Elshaer, W. Kaialy, Thermal energy storage using metal–organic framework materials, Appl. Energy. (2016), https://doi.org/10.1016/j.apenergy.2016.03.113.
[26] V. Bon, Metal-organic frameworks for energy-related applications, Curr. Opin. Green Sustain. Chem. 4 (2017) 44–49, https://doi.org/10.1016/j.cogsc.2017.02.005.
[27] P. D'Ans, E. Courbon, M. Frère, G. Descy, T. Segato, M. Degrez, Severe corrosion of steel and copper by strontium bromide in thermochemical heat storage reactors, Corros. Sci. (2018), https://doi.org/10.1016/j.corsci.2018.04.020.
[28] A. Solé, L. Miró, C. Barreneche, I. Martorell, L.F. Cabeza, Corrosion of metals and salt hydrates used for thermochemical energy storage, Renew. Energy 75 (2015) 519–523, https://doi.org/10.1016/j.renene.2014.09.059.
[29] L.G. Gordeeva, Y.I. Aristov, Composites "salt inside porous matrix" for adsorption heat transformation: a current state-of-the-art and new trends, Int. J. Low-Carbon Technol. 7 (2012) 288–302, https://doi.org/10.1093/ijlct/cts050.
[30] Y.I. Aristov, Y.A. Kovalevskaya, M.M. Tokarev, I.E. Paukov, Low temperature heat capacity of the system "silica gel-calcium chloride-water,", J. Therm. Anal. Calorim. 103 (2011) 773–778, https://doi.org/10.1007/s10973-010-0981-8.
[31] M. Tokarev, L. Gordeeva, V. Romannikov, I. Glaznev, Y. Aristov, New composite sorbent CaCl2 in mesopores for sorption cooling/heating, Int. J. Therm. Sci. 41 (2002) 470–747, https://doi.org/10.1016/S1290-0729(02)01339-X.
[32] E. Courbon, P. D'Ans, A. Permyakova, O. Skrylnyk, N. Steunou, M. Degrez, M. Frère, A new composite sorbent based on SrBr2 and silica gel for solar energy storage application with high energy storage density and stability, Appl. Energy 190 (2017) 1184–1194.
[33] L.G. Gordeeva, G. Restuccia, A. Freni, Y.I. Aristov, Water sorption on composites "LiBr in a porous carbon,", Fuel Processing Technology, (2002), pp. 225–231, https://doi.org/10.1016/S0378-3820(02)00186-8.
[34] G.T. Whiting, D. Grondin, D. Stosic, S. Bennici, A. Auroux, Zeolite-MgCl2 composites as potential long-term heat storage materials: influence of zeolite properties on heats of water sorption, Sol. Energy Mater. Sol. Cells 128 (2014) 289–295, https://doi.org/10.1016/j.solmat.2014.05.016.
[35] G. Whiting, D. Grondin, S. Bennici, A. Auroux, Heats of water sorption studies on zeolite-MgSO4 composites as potential thermochemical heat storage materials, Sol. Energy Mater. Sol. Cells 112 (2013) 112–119, https://doi.org/10.1016/j.solmat.2013.01.020.
[36] T.S. Yan, T.X. Li, J.X. Xu, R.Z. Wang, Water sorption properties, diffusion and kinetics of zeolite NaX modified by ion-exchange and salt impregnation, Int. J. Heat Mass Transf. 139 (2019) 990–999, https://doi.org/10.1016/j.ijheatmasstransfer.2019.05.080.
[37] A. Permyakova, S. Wang, E. Courbon, F. Nouar, N. Heymans, P. D'Ans, N. Barrier, P. Billemont, G. De Weireld, N. Steunou, M. Frère, C. Serre, Design of salt–metal organic framework composites for seasonal heat storage applications, J. Mater. Chem. A (2017), https://doi.org/10.1002/cssc.201700164.
[38] W. Shi, Y. Zhu, C. Shen, J. Shi, G. Xu, X. Xiao, R. Cao, Water sorption properties of functionalized MIL-101(Cr)-X (X = -NH2, –SO3H, H, –CH3, –F) based composites as thermochemical heat storage materials, Microporous Mesoporous Mater. 285 (2019) 129–136, https://doi.org/10.1016/j.micromeso.2019.05.003.
[39] P. D'Ans, E. Courbon, A. Permyakova, F. Nouar, C. Simonnet-Jégat, F. Bourdreux, L. Malet, C. Serre, M. Frère, N. Steunou, A new strontium bromide MOF composite with improved performance for solar energy storage application, J. Energy Storage 25 (2019) 100881, , https://doi.org/10.1016/j.est.2019.100881.
[40] A. Grekova, L. Gordeeva, Y. Aristov, Composite sorbents "li/Ca halogenides inside multi-wall carbon nano-tubes" for thermal energy storage, Sol. Energy Mater. Sol. Cells. 155 (2016) 176–183, https://doi.org/10.1016/j.solmat.2016.06.006.
[41] Y.I. Aristov, G. Restuccia, M.M. Tokarev, H.D. Buerger, A. Freni, Selective water sorbents for multiple applications. 11. CaCl2 confined to expanded vermiculite, React. Kinet. Catal. Lett. 71 (2000) 377–384, https://doi.org/10.1023/A:1010351815698.
[42] Y.I. Aristov, M.M. Tokarev, G. Restuccia, G. Cacciola, M.T. Aristov, Yu.I.G. Resstucia, G. Cacciola, Selective water sorbents for multiple applications, 1. CaCl2 confined in mesopores of silica gel: sorption properties, React. Kinet. Catal. Lett. 59 (1996) 325–333, https://doi.org/10.1007/BF02475434.
[43] E. Courbon, P. D'Ans, A. Permyakova, O. Skrylnyk, N. Steunou, M. Degrez, M. Frère, Further improvement of the synthesis of silica gel and CaCl2 composites: enhancement of energy storage density and stability over cycles for solar heat storage coupled with space heating applications, Sol. Energy 157 (2017) 532–541, https://

doi.org/10.1016/j.solener.2017.08.034.
[44] M. Gaeini, A.L. Rouws, J.W.O. Salari, H.A. Zondag, C.C.M. Rindt, Characterization of microencapsulated and impregnated porous host materials based on calcium chloride for thermochemical energy storage, Appl. Energy 212 (2018) 1165–1177, https://doi.org/10.1016/j.apenergy.2017.12.131.
[45] D. Mahon, P. Henshall, G. Claudio, P.C. Eames, Feasibility study of MgSO4 + zeolite based composite thermochemical energy stores charged by vacuum flat plate solar thermal collectors for seasonal thermal energy storage, Renew. Energy (2019), https://doi.org/10.1016/j.renene.2019.05.135.
[46] Y.N. Zhang, R.Z. Wang, Y.J. Zhao, T.X. Li, S.B. Riffat, N.M. Wajid, Development and thermochemical characterizations of vermiculite/SrBr2 composite sorbents for low-temperature heat storage, Energy 115 (2016) 120–128, https://doi.org/10.1016/j.energy.2016.08.108.
[47] L.G. Gordeeva, Selective water sorbents for multiple applications, 5. LiBr confined in mesopores of silica gel: sorption properties, React. Kinet. Catal. Lett. 63 (1998) 81–88, https://doi.org/10.1007/BF02475434.
[48] L.G. Gordeeva, Y.I. Aristov, Composite sorbent of methanol " LiCl in mesoporous silica gel" for adsorption cooling: dynamic optimization, Energy 36 (2011) 1273–1279, https://doi.org/10.1016/j.energy.2010.11.016.
[49] V. Brancato, L.G. Gordeeva, A.D. Grekova, A. Sapienza, S. Vasta, A. Frazzica, Y.I. Aristov, Water adsorption equilibrium and dynamics of LICL/MWCNT/PVA composite for adsorptive heat storage, Sol. Energy Mater. Sol. Cells 193 (2019) 133–140, https://doi.org/10.1016/J.SOLMAT.2019.01.001.
[50] X. Zheng, T.S. Ge, R.Z. Wang, L.M. Hu, Performance study of composite silica gels with different pore sizes and different impregnating hygroscopic salts, Chem. Eng. Sci 120 (2014) 1–9, https://doi.org/10.1016/j.ces.2014.08.047.
[51] Y. Yuan, H. Zhang, F. Yang, N. Zhang, X. Cao, Inorganic composite sorbents for water vapor sorption: a research progress, Renew. Sustain. Energy Rev. 54 (2016) 761–776, https://doi.org/10.1016/j.rser.2015.10.069.
[52] L.G. Gordeeva, I.S. Glaznev, E.V. Savchenko, V.V. Malakhov, Y.I. Aristov, Impact of phase composition on water adsorption on inorganic hybrids "salt/silica,", J. Colloid Interface Sci. 301 (2006) 685–691, https://doi.org/10.1016/j.jcis.2006.05.009.
[53] H. Wu, S. Wang, D. Zhu, Effects of impregnating variables on dynamic sorption characteristics and storage properties of composite sorbent for solar heat storage, Sol. Energy 81 (2007) 864–871, https://doi.org/10.1016/j.solener.2006.11.013.
[54] D. Zhu, H. Wu, S. Wang, Experimental study on composite silica gel supported CaCl2 sorbent for low grade heat storage, Int. J. Therm. Sci. 45 (2006) 804–813, https://doi.org/10.1016/j.ijthermalsci.2005.10.009.
[55] J.G. Ji, R.Z. Wang, L.X. Li, New composite adsorbent for solar-driven fresh water production from the atmosphere, Desalination 212 (2007) 176–182, https://doi.org/10.1016/j.desal.2006.10.008.
[56] F. Assilzadeh, S.A. Kalogirou, Y. Ali, K. Sopian, Simulation and optimization of a LiBr solar absorption cooling system with evacuated tube collectors, Renew. Energy 30 (2005) 1141–1159, https://doi.org/10.1016/j.renene.2004.09.017.
[57] Z. Li, X. Ye, J. Liu, Performance analysis of solar air cooled double effect LiBr/H2O absorption cooling system in subtropical city, Energy Convers. Manag. 85 (2014) 302–312, https://doi.org/10.1016/j.enconman.2014.05.095.
[58] D.S. Kim, C.A. Infante Ferreira, Air-cooled LiBr-water absorption chillers for solar air conditioning in extremely hot weathers, Energy Convers. Manag. 50 (2009) 1018–1025, https://doi.org/10.1016/j.enconman.2008.12.021.
[59] K.E. N'Tsoukpoe, N. Le Pierrès, L. Luo, Numerical dynamic simulation and analysis of a lithium bromide/water long-term solar heat storage system, Energy 37 (2012) 346–358, https://doi.org/10.1016/j.energy.2011.11.020.
[60] W. Rivera, A. Huicochea, R.J. Romero, A. Lozano, Experimental assessment of double-absorption heat transformer operating with H2O/LiBr, Appl. Therm. Eng. 132 (2018) 432–440, https://doi.org/10.1016/J.APPLTHERMALENG.2017.12.117.
[61] H. Zhang, D. Yin, S. You, W. Zheng, S. Wei, Experimental investigation of heat and mass transfer in a LiBr-H2O solution falling film absorber on horizontal tubes: comprehensive effects of tube types and surfactants, Appl. Therm. Eng. 146 (2019) 203–211, https://doi.org/10.1016/J.APPLTHERMALENG.2018.09.127.
[62] F. Asfand, M. Bourouis, Estimation of differential heat of dilution for aqueous lithium (bromide, iodide, nitrate, chloride) solution and aqueous (lithium, potassium, sodium) nitrate solution used in absorption cooling systems, Int. J. Refrig. 71 (2016) 18–25, https://doi.org/10.1016/j.ijrefrig.2016.08.008.
[63] P.A.J. Donkers, L.C. Sögütoglu, H.P. Huinink, H.R. Fischer, O.C.G. Adan, A review of salt hydrates for seasonal heat storage in domestic applications, Appl. Energy 199 (2017) 45–68, https://doi.org/10.1016/j.apenergy.2017.04.080.
[64] S. Glöser, L. Tercero Espinoza, C. Gandenberger, M. Faulstich, Raw material criticality in the context of classical risk assessment, Resour. Policy 44 (2015) 35–46, https://doi.org/10.1016/j.resourpol.2014.12.003.
[65] O. Skrylnyk, E. Courbon, N. Heymans, M. Frère, J. Bougard, G. Descy, Performance characterization of salt-in-silica composite materials for seasonal energy storage design, J. Energy Storage 19 (2018) 320–336, https://doi.org/10.1016/j.est.2018.08.015.
[66] Courbon Skrylnyk, Frère Heymans, Combined solar thermochemical solid/gas energy storage process for domestic thermal applications: analysis of global performance, Appl. Sci. 9 (2019) 1946, https://doi.org/10.3390/app9091946.
[67] L.G. Gordeeva, A. Freni, T.A. Krieger, G. Restuccia, Y.I. Aristov, Composites "lithium halides in silica gel pores": methanol sorption equilibrium, Microporous Mesoporous Mater. 112 (2008) 254–261, https://doi.org/10.1016/j.micromeso.2007.09.040.
[68] O. Haut, M. Secula, I. Solomon, M. Ioan, Separation of water vapors from air by sorption on some composite materials, Sci. Study Res. Chem. Chem. Eng. Biotechnol. Food Ind. 14 (2013) 113–118.
[69] J. Mrowiec-Bialon, a.I. Lachowski, a.B. Jarzebski, L.G. Gordeeva, Y.A. Aristov, SiO2-LiBr nanocomposite sol-gel adsorbents of water vapor: preparation and properties, J. Colloid Interface Sci. 218 (1999) 500–503.
[70] Y.Y. Tanashev, A.V. Krainov, Y.I. Aristov, Thermal conductivity of composite sorbents "salt in porous matrix" for heat storage and transformation, Appl. Therm. Eng. 61 (2013) 401–407, https://doi.org/10.1016/j.applthermaleng.2013.08.022.
[71] E. Courbon, M. Frère, N. Heymans, P. D'Ans, Hygroscopic Composite Material, WO2015197788, 2015.
[72] M. Polanyi, Principles of the potential theory of adsorption, Elektrochem 35 (1929) 431.
[73] M. Polanyi, Theories of the adsorption of gases. A general survey and some general remarks, Trans. Faraday Soc. 28 (1932) 316.
[74] D.D. Do, Adsorption analysis: equilibria and kinetics, Series on Chemical Engineering 2 Imperial C, 1998.